Available on CMS information server

CMS NOTE 2007/027

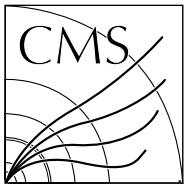

The Compact Muon Solenoid Experiment

CMS Note

Mailing address: CMS CERN, CH-1211 GENEVA 23, Switzerland

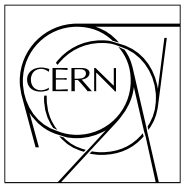

4 October 2007

Timing of the CMS tracker. Study of module properties.

C. Delaere, L. Mirabito

CERN, Geneva, Switzerland

Abstract

One of the crucial aspects of the commissioning of the CMS silicon tracker will be the absolute timing of each module, to accommodate both the delays introduced by the hardware configuration and the effects due to the time-of-flight of particles. The goal is to be optimally synchronized with the bunch crossing to maximize the signal height while minimizing the number of remnant hits from the adjacent bunch crossings.

In the present note, a procedure to reach this goal is deduced from the analysis of the results obtained with a simple test setup. Emphasis is put on the parametrization of the pulse shape and on the effect of capacitive coupling between adjacent strips. It is shown that the pulse from the leading strip must be used as a reference during the timing procedure, in order to have a symmetric efficiency over consecutive bunch crossings and to avoid fake clusters.

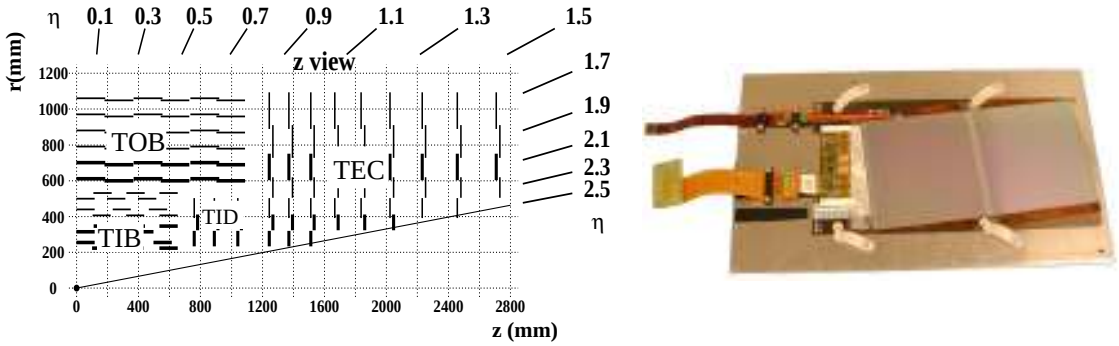

(a) (b)

Figure 1: (a) Sketch of the tracker layout (1/4 of the r-z view); (b) a TOB module on its aluminum transport plate.

1 Introduction

The CMS silicon strip tracker is the largest device of its type ever built. It is divided into four main subsystems: the Inner Barrel (TIB), the Outer Barrel (TOB), the Inner Disks (TID) and the Endcaps (TEC) (Figure 1). There are 24244 single-sided micro-strip sensors covering an active area of 198m^2. Throughout the tracker, the strip pitch varies from the inner to the outer layers (from 80μm to 205μm) in order to cope with the anticipated occupancy and to grant a good two-hit resolution [1].

The size of the device has led to a design where the basic unit, called a module, houses the silicon sensors and the readout electronics. Charges are collected every 25ns and stored in an analog pipeline (APV25) on the front-end hybrid [2]. The APV25 chip also contains a CR-RC shaper and a deconvolution circuit to reduce the signal width (see Section 3). The read-out can be performed either with or without the deconvolution, depending on the pile-up conditions. The two modes of operation are respectively called deconvolution mode and peak mode.

One aspect of the commissioning of the CMS silicon tracker will be the absolute timing of each module from data, to accommodate both the delays introduced by the hardware configuration and the effects due to the time-of-flight of particles. The objective is to be optimally synchronized with the bunch crossing to maximize the efficiency while minimizing the number of fake hits from adjacent bunch crossings. This aspect is critical due to the high frequency of interactions at the LHC (nearly 40MHz).

The CMS tracker is not able to produce a trigger signal by its own. An external (Level-1) trigger generated from the information collected by other subdetectors is fed by dedicated optical links from the front-end controllers to the APV25 chips. Upon reception of a trigger signal, data for the corresponding bunch crossing is read from the pipeline and sent to the front-end drivers (FED) via analog optical links. This is where the analog-to-digital conversion is done. The differences in length of these analog lines are compensated by programmable delays at the input of the FEDs. FED delays are set according to the information stored in the construction database.

To achieve the synchronization of the electronics a dedicated programmable delay is available in the Phase-Locked Loop (PLL) that is embedded in the front-end electronic of each module. It allows to shift the clock and trigger signals by steps of 1.04 ns. The global latency with respect to the central trigger is compensated by the "latency" parameter of each APV25 chip. That parameter defines an offset in the APV25 analog pipeline by steps of 25ns.

The chip outputs a synchronization pulse called 'tick mark' every 35 clock cycles when there is no data to read out. The tick mark can be used to first synchronize all modules with each other to compensate for the length of optical and electrical links as well as for the electronics latency. This is done adjusting the PLL delays. The delay settings determined in this way have to be corrected to take into account the time of flight from the interaction point to each module as well as the latency with respect to the trigger. If the first is known from the geometry, the latter can only be determined by performing a latency scan. To guarantee optimal synchronization in a minimal amount of time, the latency scan is performed in two steps. In a first round, a rough global scan is performed in steps of 25ns using the APV25 latency. This allows the correct bunch crossing to be located. A finer scan is then performed per detector layer, taking into account all possible effects. The aim is to achieve a precision of 1ns by using hits from selected tracks and readjusting the PLL delays. The commissioning sequence can therefore be sketched as follows.

1. Tune the PLL delays to synchronize all the tracker modules using the tick marks, i.e. guarantee that the clock is arriving synchronously on all tracker modules. This is done in one go for all the tracker.
2. Correct that tuning to take into account the theoretical time-of-flight. For that purpose, particles are assumed to propagate straight from the nominal interaction point to the center of the module.
3. Perform a rough global latency scan with respect to the central trigger, i.e. find the global shift between the tracker trigger and the central one. This is done tuning the APV25 latency parameter. This is done in one go for all the tracker.
4. Perform a fine latency scan by retuning the PLL delays. This is done per detector layer to ensure that each reconstructed track crosses the considered subset once, being almost unaffected by the commissioning procedure.

The aim of the present note is to study the key module properties that will impact the fine latency scan and to establish the optimal procedure. If the pulse shape is not nominal, the delay between the central trigger and the maximum of the signal is significantly affected. Prior to the actual timing, the response of each module has therefore to be tuned to match the specifications. This can be done by adjusting the CR-RC shaper input FET current bias (ISHA) and the shaper feedback voltage bias (VFS) individually on each APV25 chip. Effects impacting the charge collection, like the charge sharing and the capacitive coupling, must also be considered.

The present note is organized as follows. In section 2, the experimental setup will be briefly described. In section 3, it will be shown how to describe the APV response in terms of CR-RC curves in peak mode, and how it adapts to deconvoluted mode. In section 4, that description will be used to choose the working point for the ISHA and VFS parameters. In section 5, the actual procedure for tuning the delays between modules will finally be described.

2 Experimental setup

In order to study timing at the level of the module, measurements were done with a single TOB module exposed to the light of a pulsed laser. This module has two 500μm thick silicon sensors and four APV chips. Readout control (Figure 2) consists of a Front-End Controller (FEC) PMC board, optically connected to a Control Chip Unit (CCU). The CCU propagates the 40MHz clock and trigger signals to the front-end. It also provides control lines to the front-end chips. The analog readout is done optically by a 40MHz flash ADC PMC card (FED-PMC). A detailed description of the readout system can be found in [3]. The clock and trigger signals are generated by a Trigger Sequence card [4] also triggering the laser pulser.

The laser setup consists of one 1060nm laser triggered by a narrow (1.6ns) pulse. With the help of a spherical lens, the laser can be focused on a single strip, or set to hit more strips. It can also be aligned with a precision of 10μm, and the intensity can be tuned to produce a MIP pulse. Data were obtained with this setup for different modes of operation of the front-end electronics in order to study the pulse shape in the time domain on individual strips.

A single PC holds the TSC, FEC and FED PCI cards and runs the XDAQ-based[5] data acquisition program[6].

3 Description the module response

A typical pulse shape obtained using the experimental setup just described is presented in Figure 3. Ideally, the analytical form of the pulse shape in peak mode is the transfer function in the time domain of a CR-RC:

$$S_{\text{peak}}(t) \propto \frac{t}{\tau} e^{-t/\tau}, \tag{1}$$

where τ is the rise time, and the time t is positive.

The pulse read from the silicon lasts about 300ns, which is large with respect to the 25ns time that separate two bunch crossings. The deconvolution method should ideally give a full efficiency and maximum signal for the trigger bunch crossing and no signal for previous and next bunch crossings. The

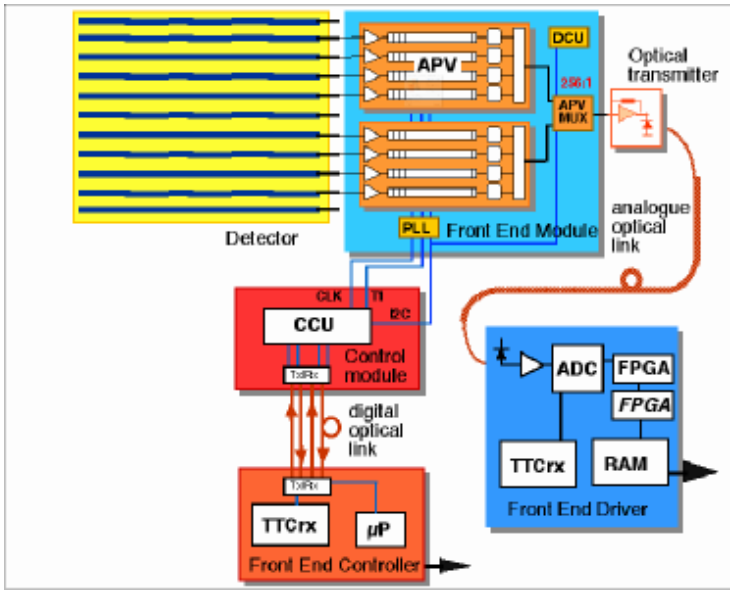

Figure 2: Schematic diagram of the readout and control system.

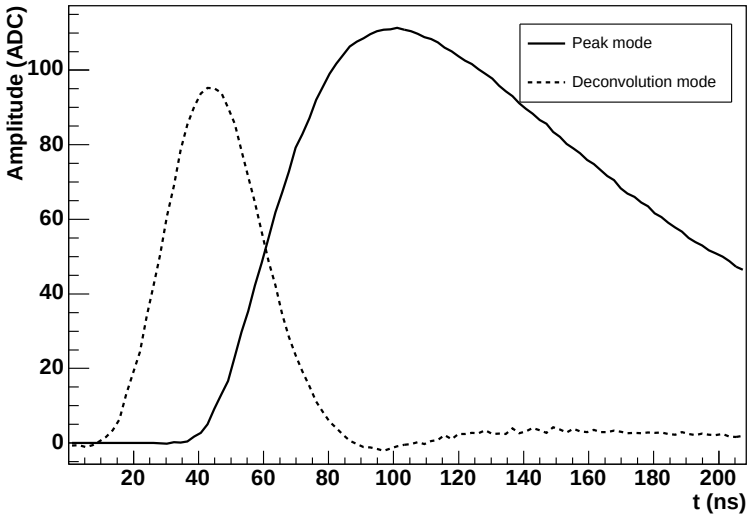

Figure 3: Pulse shape in peak and deconvolution mode for a TOB module. Data are obtained using the setup described in 2.

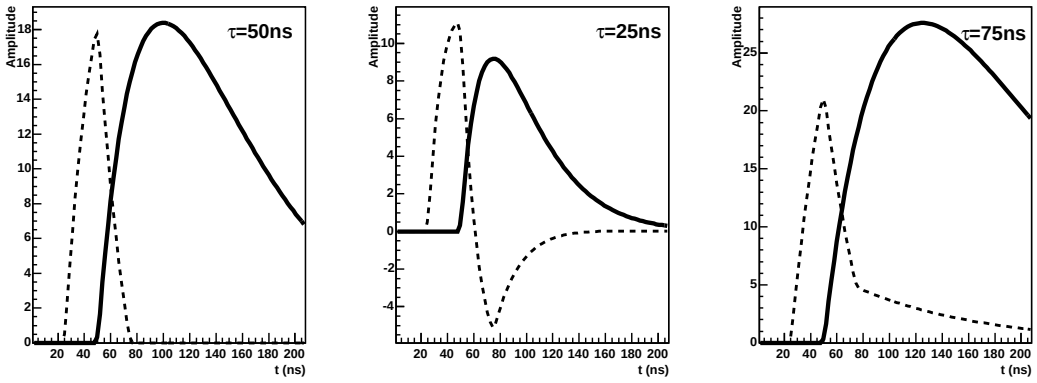

Figure 4: Ideal response, both in peak mode (solid) and in deconvolution (dashed) mode, for three values of the rise time. For the nominal rise time of 50ns, the deconvoluted curve is a RC curve.

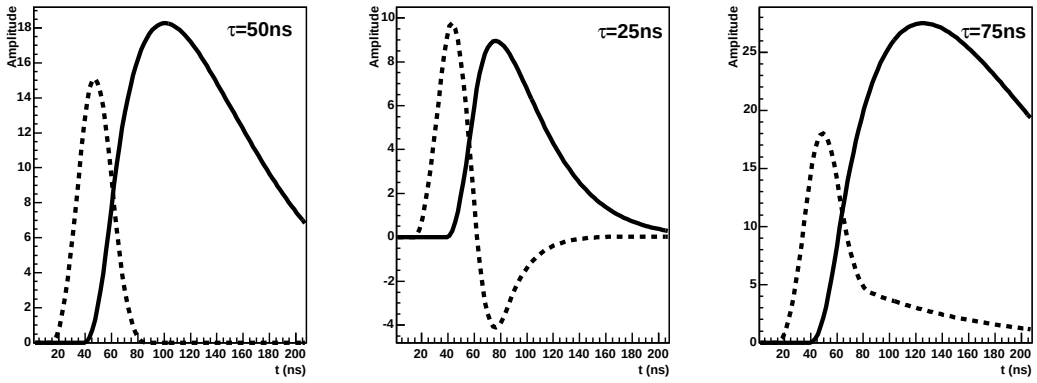

Figure 5: Pulse shape obtained by smearing the ideal response by 16ns, both in peak mode (dashed) and in deconvolution mode (dashed), and for three values of the rise time.

pulse shape in deconvolution mode is obtained from the one in peak mode by applying the following deconvolution algorithm[7], optimized for a rise time of 50ns:

$$S_{\text{deconv}}(t) = 1.2131 S_{\text{peak}}(t - 25ns) - 1.4715 S_{\text{peak}}(t) + 0.4463 S_{\text{peak}}(t + 25ns). \quad (2)$$

This function is presented in Figure 4, together with the original CR-RC function as a function of the actual τ value. Another significant effect that has to be considered is the drift time of charge carriers in the bulk of the silicon sensor. In particular, holes need several tens of nanoseconds to travel over the 320 or 500μm of the sensor. The exact time needed depends on the applied bias and on the doping density, but also on the temperature. An empirical relation[8] obtained by fitting experimental values is

$$\begin{aligned} \mathrm{t} &= \frac{\mathrm{H}^2}{\mu_h \mathrm{V}} & (3) \\ \mu_h &= 54.3\left(\frac{\mathrm{T}}{300}\right)^{0.57} + \frac{1.35 \times 10^8 \mathrm{T}^{2.23}}{1 + \frac{\mathrm{N}}{2.35 \times 10^{17} (\frac{\mathrm{T}}{300})^{2.4}} 0.88 (\frac{\mathrm{T}}{300})^{0.146}}, & (4) \end{aligned}$$

where t is the maximum drift time, μ_h is the hole mobility, N is the doping concentration, T is the temperature in degree Kelvin, H is the thickness and V is the bias applied to the module. In order to take into account the drift time of holes in the silicon, the analytical form (1) has to be smeared over the drift time. That smearing is performed by convoluting the CR-RC curve with a normalized rectangle function:

$$\begin{aligned} \widetilde{S}_{\text{peak}}(t) &= \int_{-\infty}^{+\infty} S_{\text{peak}}(t') f(t')\, dt'; \qquad f(t') = \frac{2}{\delta} \Pi\left(\frac{t' - t}{\delta}\right) \\ &= \frac{1}{\delta} \int_{t-\delta/2}^{t+\delta/2} S_{\text{peak}}(t')\, dt'. & (5) \end{aligned}$$

In these expressions, the width of the rectangle function corresponds to the maximum drift time. Since the deconvolution algorithm is linear, deconvoluting a smeared CR-RC also reproduces the smeared pulse shape before the CR-RC convolution, as it is shown in Figure 5.

$$\begin{aligned} \widetilde{S}_{\text{deconv}}(t) &= \int_{-\infty}^{+\infty} S_{\text{deconv}}(t') f(t')\, dt' \\ &= 1.2131 \widetilde{S}_{\text{peak}}(t - 25ns) - 1.4715 \widetilde{S}_{\text{peak}}(t) + 0.4463 \widetilde{S}_{\text{peak}}(t + 25ns). & (6) \end{aligned}$$

The result of the smearing does not depend strongly on the exact form of the smearing function $f(t')$. Only the smearing time δ is critical. The position of the signal is not affected by the smearing time. The precise position of the maximum is only slightly affected for very small values of the smearing time (below 10ns) as the curve becomes more and more symmetric when the smearing time increases.

The dependence of the drift time on the bias voltage is demonstrated in Figure 6, where the optimal smearing time obtained by fitting the pulse shape measured for different bias voltages is shown. The $1/\mathrm{V}$ dependence is clearly seen. The slope corresponds to a hole mobility of $45.7 \frac{\mu\mathrm{m}^2}{\mathrm{Vns}}$, perfectly compatible with the doping concentration of CMS silicon sensors, while the constant term is compatible with the length of the laser pulse. From the same fit it appears that the contribution of the electronics to the smearing time is small. For small bias voltage, the detector is not fully depleted which compensates the smaller mobility of charge carriers. Therefore, the drift time does not follow the power law below 200 V anymore.

In addition to the signal resulting from the collection of charges produced in the bulk of the sensor, there is a signal induced on adjacent strips because of capacitive coupling. The induced signal is characterized by a reduced amplitude and a smaller rise time, as can be seen in Figure 7. In that Figure, dots are representing measurements while the line results from the fit using equation 6. The induced signal can be parametrized by a (deconvoluted) smeared CR-RC curve with the following characteristics: the amplitude A and the rise time τ on the nearby strips are given approximately by

$$A = A_0 * 0.4^n, \quad (7)$$

$$\tau = \tau_0 \frac{1}{1 + 1.26n}. \quad (8)$$

where n is the distance to the hit strip, in units of pitch, while A_0 and τ_0 are respectively the amplitude and the rise time of the signal on the hit strip. If charges are distributed over more than one strip, the

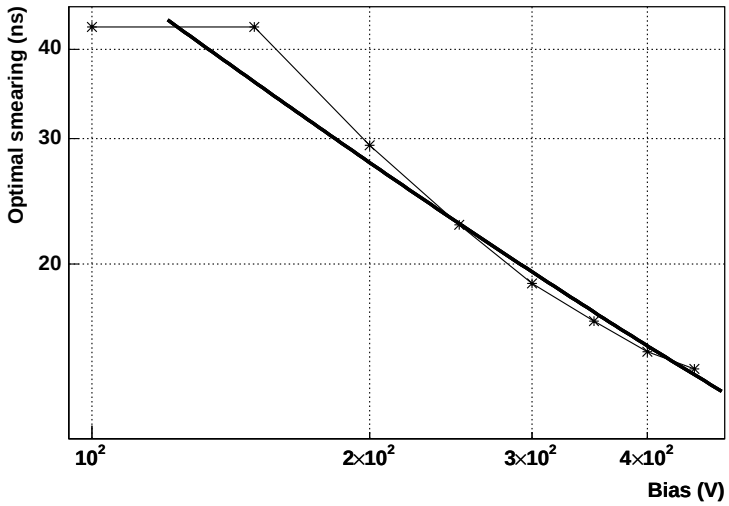

Figure 6: Optimal smearing time (reflecting the drift time in the pulse shape parametrization) obtained by fitting the delay curve for different bias voltages. The thick curve is a fit to a hole mobility of $45.7\frac{\mu m^2}{Vns}$, performed on the range $[200V, 500V]$.

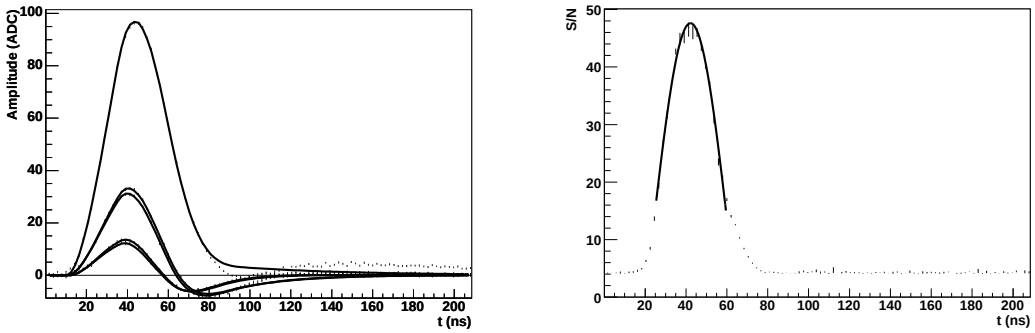

(a) (b)

Figure 7: (a) Response of a TOB module hit on a single strip by a focused laser. The signal on the hit strip is shown in deconvolution mode together with the signal from the two adjacent strips on each side. (b) Signal-to-noise behavior for the corresponding reconstructed cluster in deconvolution mode. The cluster signal is the sum of the signal on all its strips while the cluster noise is defined as the quadratic sum of the noise of all strips contributing to the cluster.

response of each strip is a combination of the signal expected directly and of the signal induced by capacitive coupling. It results in a slightly broader peak. In the same figure, the signal-to-noise behavior as a function of time is shown for the corresponding reconstructed cluster obtained by collecting adjacent strips with a signal to noise ratio higher than four and imposing a total signal-to-noise ratio larger than two for the resulting cluster.

4 Optimal module parameters

Among the parameters of the APVs, ISHA and VFS are the two values that control the pulse shape. In particular, VFS has a strong effect on the rise time and fall time in peak mode. It has therefore an impact on the tail in deconvolution mode, causing undershoots or non-vanishing signals when the value is wrongly set. At the same time, ISHA affects the amplitude in deconvolution mode with a marginal impact on the rise time. Figure 8 shows how the pulse shape depends on these two parameters both in peak and deconvolution mode. The fitted curve corresponding to the optimal choice is represented as a continuous line.

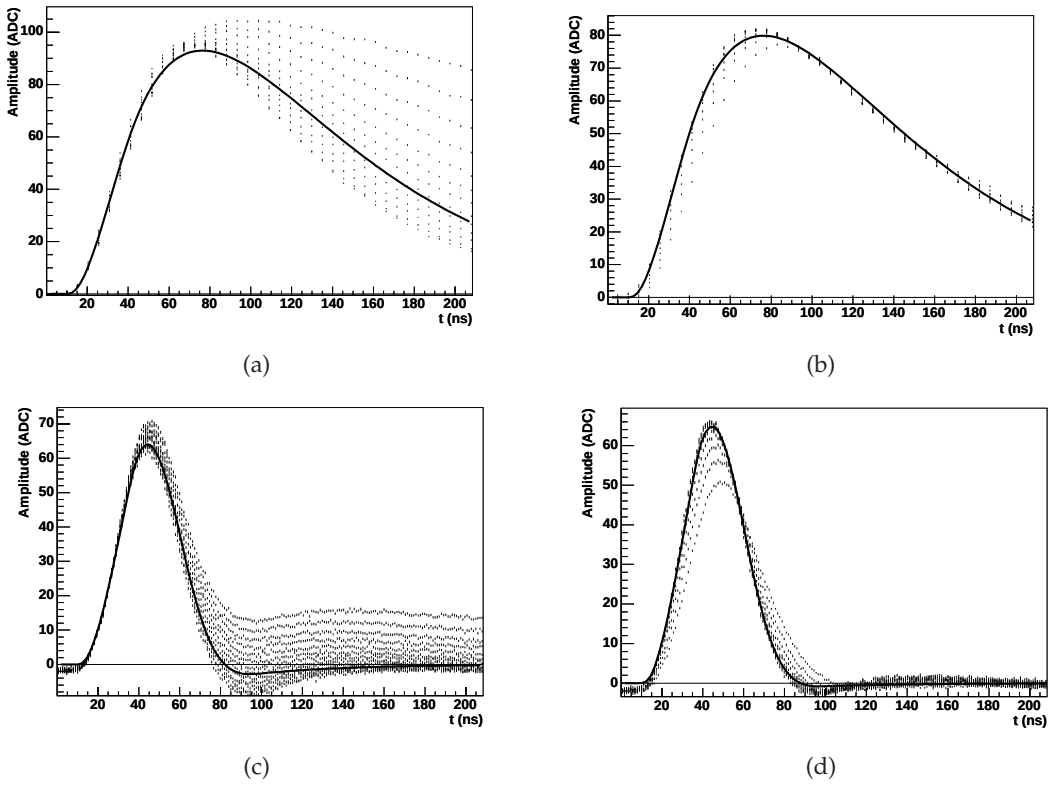

Figure 8: Pulse shape obtained in peak (a and b) and deconvolution (c and d) mode for different values of ISHA and VFS. The pulse obtained for different settings are shown as dotted curves, and the fit of the curve corresponding to the recommended parameters (VFS=50, ISHA=80) is drawn as a continuous line. In plots a and c, VFS is varied from 0 to 120. In plots b and d, ISHA is varied from 30 to 100.

The optimal value of these parameters can be automatically extracted from fits of the pulse shape. In particular, requesting a good fit with a rise time of 50ns will fix VFS. ISHA has a more global effect on the pulse shape, and an optimal value can be obtained by minimizing the χ^2 of the fit of the pulse shape with an ideal RC-CR curve. The optimal values will depend on the detector capacitance, and hence on the geometry of the sensor.

5 Optimal synchronization

Figure 7 shows the response of a TOB module hit on a single strip by a focused laser. In addition to the signal on the hit strip, there is a signal induced on the nearby strips by capacitive coupling. That induced signal has a shorter rise time, that causes the undershoot observed in deconvolution mode. One important consequence is that the signal response for the reconstructed cluster has a maximum in advance by a few nanoseconds (typically 2ns) with respect to the hit strip. Tuning the module on the maximum of the leading strip or on the maximum of the cluster will therefore give different results. In the case of a single hit strip, for a cluster signal normalized to a signal-to-noise of 20 and for a S/N cut of 4, the cluster efficiency for the bunch crossing following the interaction is still 33%, while it is zero in the bunch crossing just before the interaction (Figure 9). It appears that tuning the module on the leading strip is the only method that gives a symmetric efficiency around the nominal bunch crossing. In that case, the efficiency is also only of the order of a few permil in the two adjacent bunch crossings. For completeness, Figures 10 and 11 show the response of a TOB module hit on two and three strips, respectively. Table 1 shows the delay between the maximum of the signal on the leading strip and on the cluster for different numbers of hit strips. As can be seen, the effect does not depend strongly on the configuration of the cluster.

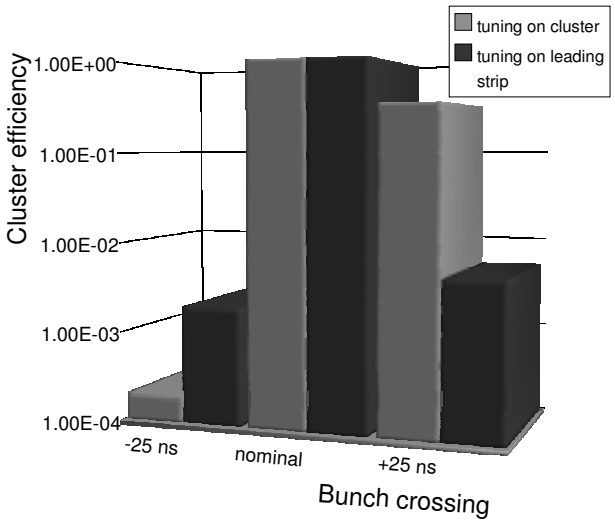

Figure 9: Typical cluster efficiency obtained using a synchronization on the cluster or on the leading strip. The efficiency is more symmetric when the leading strip is used as reference.

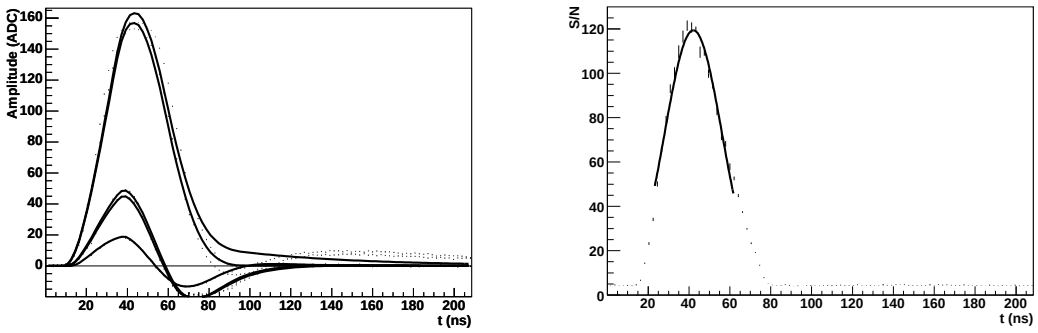

(a) (b)

Figure 10: (a) Response of a TOB module hit on two strips by a focused laser. The signal on the hit strips is shown in deconvolution mode together with the signal from the adjacent strip on each side. (b) Signal-to-noise behavior for the corresponding reconstructed cluster in deconvolution mode. The cluster signal is the sum of the signal on all its strips while the cluster noise is defined as the quadratic sum of the strip noise over the cluster.

Table 1: Mean cluster signal-to-noise ratio for different configurations of hits, when tuning the delay on the cluster maximum or on the strip maximum. The signal-to-noise ratio is shown in the nominal bunch crossing, and in the bunch crossing before and after. The delay between the maximum of the signal on the leading strip and on the cluster is also presented, together with the asymmetry, computed from the signal-to-noise ratio in the bunch crossing before (R_-) and after (R_+) the nominal bunch crossing as $(R_+ - R_-)/(R_+ + R_-)$.

Number of hit strip(s)	Delay (ns)	Tuning on	Mean cluster signal-to-noise ratio			
			-25ns	Nominal	+25ns	asymmetry
1	2.1	cluster	1.9	20	3.8	0.5
		strip	2.2	19.7	3.1	0.1
2	1.5	cluster	1.6	20	4.9	0.5
		strip	3.5	19.5	4.1	0.1
3	1.4	cluster	1.0	20	2.5	0.4
		strip	1.4	19.7	1.7	0.1

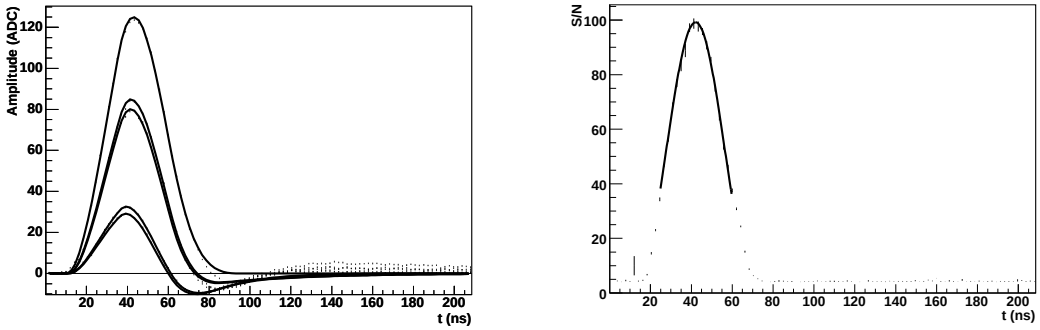

(a) (b)

Figure 11: (a) Response of a TOB module hit on three strips by a slightly defocused laser. The signal on the hit strips is shown in deconvolution mode together with the signal from the adjacent strip on each side. (b) Signal-to-noise behavior for the corresponding reconstructed cluster in deconvolution mode. The cluster signal is the sum of the signal on all its strips while the cluster noise is defined as the quadratic sum of the strip noise over the cluster.

These results have a crucial impact on the fine latency scan that is part of the commissioning sequence. The recommended procedure is:

1. Switch to deconvolution mode for a given layer to have the best time resolution near the maximum of the pulse.
2. Accumulate events and reconstruct tracks.
3. Record the charge deposited on the leading strip in the vicinity of the crossing point between each track and the studied layer.
4. Iterate while scanning the PLL delay by steps of one or two nanoseconds.
5. Fit the distribution obtained with a deconvoluted smeared CR-RC curve.
6. Set the delay to match the maximum and continue with another layer.

The efficiency of this procedure will depend on the statistics accumulated for each layer, on the track sample used and on the choice of steps during the delay scan. These issues are being worked out but are beyond the scope of the present note.

6 Summary and outlook

In the present note, we showed how the pulse shape from a module can be described using (deconvoluted) CR-RC functions once a smearing time corresponding to the drift time of holes in the silicon is introduced. The parameters extracted from the fit are mainly the rise time, the latency with respect to the trigger, and the drift time of holes in the bulk of the sensor. Using this information, the working parameters of each module can be adjusted.

Capacitive coupling between adjacent strips induces a fast signal that has a significant impact on the cluster reconstruction. We showed that it is crucial to use the maximum of the pulse from the leading strip as a reference during the timing procedure, in order to have a symmetric efficiency over consecutive bunch crossings and to avoid fake clusters.

Given the presented results, a commissioning sequence has been sketched. The details of this procedure are being worked on, including the choice of the most suitable track sample and the estimation of the time needed to accumulate the needed statistics.

References

[1] CMS collaboration, *"Tracker Technical Design Report"*, CERN/LHCC 98-6; April 1998; and CMS collaboration, *"Addendum to the CMS Tracker TDR"*, CERN/LHCC 2000-016, February 2000.

[2] L.Jones et al., *"The APV25 deep sub micron readout chip for CMS channels detectors"*, Proceedings of 5th workshop on Chips electronics for LHC experiments,CERN/LHCC/99-09,162-166.

[3] J. Bernardini et al., *"Response of the APV Readout Chip to Laser-Simulated, Highly Ionizing Interactions"*, CMS NOTE-2004/022.

[4] M. Ageron et al., *"The trigger seqencer card users's manual"*, http://lyoinfo.in2p3.fr/cms/tsc/tsc03.pdf

[5] J.Gutleber et al., *"Architectural Software Support for Processing Clusters"*, IEEE International Conference on Cluster Computing (Cluster 2000), November 28 - December 2, 2000, Chemnitz, Germany, IEEE Conference Proceedings.

[6] R.Bainbridge et al, *"Software for the CMS Strip Tracker Data Acquisition System"*, Proceedings of the Computing in High Energy Physics conference, 2007.

[7] S. Gadomski et al., *"The deconvolution method of fast pulse shaping at hadron colliders"*, Nuclear Instruments and Methods A320 (1992) 217-227.

[8] Bart Van Zeghbroeck, *"Principles of Semiconductor Devices"*, Colarado University (2004).